CHALMERS

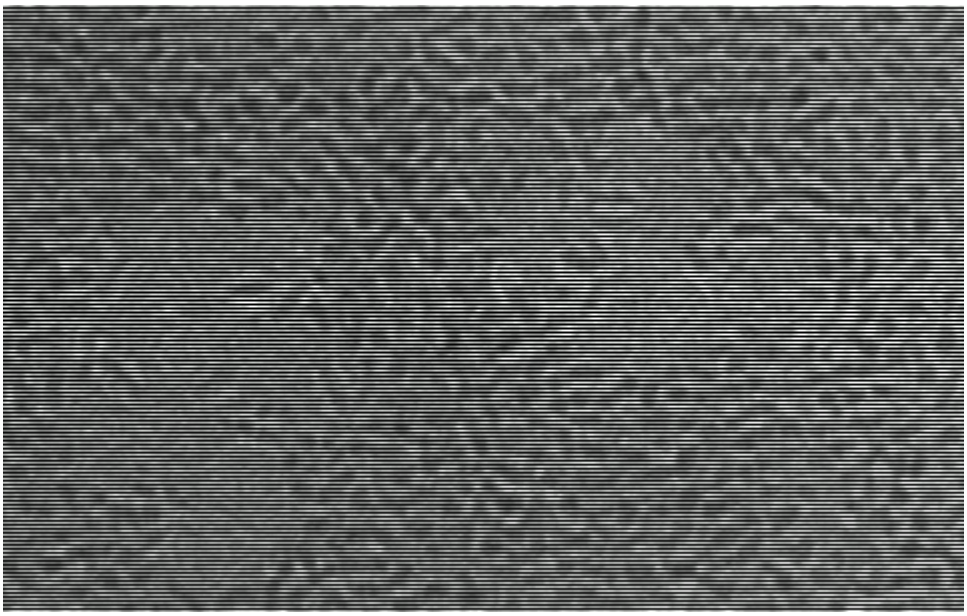

# Radioactively Labeled Titania Nanoparticles for Skin Penetration

*Master of Science Thesis in Materials Chemistry and Nanotechnology*

Kim Bini

Department of Chemical and Biological Engineering
CHALMERS UNIVERSITY OF TECHNOLOGY
Göteborg, Sweden, 2013

**Radioactively labeled titania nanoparticles for skin penetration**

Kim Bini
Department of Chemical and Biological Engineering
CHALMERS UNIVERSITY OF TECHNOLOGY
Gothenburg, Sweden, 2013

# Abstract

Titanium dioxide, a.k.a. titania, is widely used in many applications due to its unique properties. It is a photocatalytically active material, which upon absorption of sunlight can catalyze chemical reactions. It also possesses a high refractive index resulting in its common use in paints, cosmetics and sunscreens. In several of these above-mentioned applications, the desired nature of titania is in the form of nanoparticles. One risk when applying skin products containing titania nanoparticles or handling titania nanoparticles at workplaces is that they might penetrate into or through the skin. Since the skin is one of our most important biological barriers it is important to know whether such particles can enter our bodies.

This study aims to produce radioactively labeled nanosized titania particles with varied size and shape, apply them to excised skin and then analyze the skin penetration using autoradiography. Two different methods were tested for the formation of desired titania nanoparticles. One utilized low-temperature hydrolysis of titanium tetrachloride based on the work of Jenny Perez Holmberg, while the other synthetic route, which suggested by *Zhang et al*., employed controlled aminolysis of titanium isopropoxide at high temperature. Due to difficulties in forming discrete and dispersed titania particles with the first method, the latter with possibility of tuning particle shape was adopted. Since titanium lacks good nuclides for autoradiography, 10 atomic% was substituted by hafnium. Three types of hafnium doped titania nanoparticles with varied aspect ratio, presumably 12nm × 2nm rods, 30nm × 2nm rods and 2.3 nm spheres, were synthesized by adjusting reaction conditions. As-prepared nanoparticles were characterized using mainly TEM and DLS. However, due to the small dimension of the particles and the technical limitation of accessed instruments, the exact morphology of the product is not conclusive. The presence of hafnium in as-synthesized particles was verified using SEM/TEM coupled with EDX.

The hafnium doped titania particles will be irradiated by neutron radiation, which will yield certain nuclides emitting suitable radiation for autoradiography. The obtained particles will be formulated in o/w microemulsion, and then applied onto excised human skin for a predetermined amount of time and the penetration will be evaluated with autoradiography.

# Abbreviations

| | |
|---|---|
| NP | Nanoparticle |
| Hf | Hafnium |
| DLS | Dynamic Light Scattering |
| TEM | Transmission Electron Microscopy |
| SEM | Scanning Electron Microscopy |
| EDX (EDS) | Energy Dispersive X-ray Spectroscopy |
| XRD | X-ray diffraction |
| $TiO_2$ | Titanium Dioxide, titania |
| TIP | Titanium isopropoxide |
| $TiCl_4$ | Titanium tetrachloride |
| Hf | Hafnium |
| HfIP | Hafnium isopropoxide |
| OLA | Oleic Acid |
| OA | Oleylamine |
| 1-ODE | 1-octadecene |
| nm | Nanometer ($10^{-9}$m) |

# Acknowledgements

First and foremost I would like to thank Chlor for all her help and the endless TEM runs! I would also like to thank Martin Andersson for this project and all the Gaz. I wish them both good luck in the continuation of this project!

I would also like to thank my girlfriend Maria and my parents Dag and Görel for all their loving support!

# Contents

# Introduction

Nanotechnology is quickly becoming an incredibly important field of science and its economic impact is tremendous. It is already utilized in many everyday items such as sporting goods, electronics, clothing and cosmetics. Nanomaterials have always been present in nature, however it is only recently that we have started intentionally engineering them (Cademartiri, 2009). With this science comes an entirely new field of safety issues not present in ordinary materials science. As a common compound in cosmetics and sunscreen lotions, titanium dioxide acts as a physical sunscreen, reflecting the light and also absorbing UV-light, thus protecting the skin (Schulz, 2002). Titanium dioxide is generally seen as a harmless compound and has been widely used in many everyday products, but in the form of nanoparticles (NP) the safety is far less guaranteed. For example, $TiO_2$ NPs have shown some phototoxic effect when they are exposed to UV radiation (Sanders, 2012).

The human skin is an incredibly important barrier to the surrounding environment. It protects us from external stress, acts as a heat insulator and limits fluid loss (Krug, 2011). It also acts as a physical and chemical barrier. It has been shown to be an effective barrier against uptake of many types of nanoparticles, due in part to its ability to continually regenerate from the inside and exfoliate the outermost layer of old skin (Krug, 2011). Due to the widespread usage of $TiO_2$ NPs in cosmetics and sunscreens it is crucial to know the skin penetrating properties and toxicity of them. The current knowledge of this is not complete, especially for particles in the sub 10nm range (Krug, 2011). A common way to test if something can permeate human skin is to use surgically excised skin; one source of this skin is as a leftover from breast reduction operations.

One problem with NPs is that they are very small and so a good way to localize them is needed. There are many ways of tracking NPs, for example, fluorescent dyes can be used to decorate the particle surface, which enables the visualization by fluorescent microscopy (Thurn, 2009). Furthermore, particles with a gold or silver core could be tracked by utilizing plasmon resonance of the core material (Lee, 2012). Another method includes usage of quantum dots, which are semiconducting nanoparticles with a band gap, which makes them able to absorb a wide spectrum of light and emit a narrow one (Mortensen, 2008). A powerful and commonly used method is autoradiography, which uses emissions from radioactive decay

as a precise and easily detected signal. To produce radioactive particles, it is possible to either use radioactive reagent during the synthesis or to irradiate them afterwards.

# Aims

This master's thesis aims to develop a reliable synthesis route to produce hafnium doped $TiO_2$ NPs with customizable size and shape. These particles will become radioactive by neutron radiation, so that they can be used for skin permeation studies and detectable by autoradiography.

# Theoretical background

## Nanotechnology

Nanotechnology is growing massively. The value of nanostructured materials is becoming clearer and clearer as research on them proceeds, but what is so special about them? A nanostructured material is defined as a material with features in the nanometer scale, roughly $10^{-9}$ to $10^{-6}$ m. It can have features in zero, one, two or three dimensions e.g. spheres, wires, sheets or porous materials (Cademartiri, 2009). This size range gives rise to mesophenomena in between ordinary Newtonian mechanics and quantum mechanics (Cademartiri, 2009). It can also give an enormously high available surface area, which is important in many cases. These materials can show a very high reactivity, which can make them very useful, but also potentially toxic. If a small variation in particle size, shape or surface chemistry can give large effects in material properties, it is incredibly hard to study all variations for toxicity. This has led to a completely new field in itself; nanotoxicology, the study of toxic properties of nanoscale materials. Due to the rapid development of nanotechnology and the not quite as rapid toxicological assessment of engineered nanomaterials, there is a large knowledge gap to fill to ensure safe usage of nanomaterials (Nel, 2006).

## Titanium dioxide

Titanium dioxide, $TiO_2$, is an oxidized state of titanium, which has sparked much interest due to several useful and uncommon properties. These properties include thermal and chemical stability, low intrinsic toxicity, high refractive index and high photocatalytic activity, especially in its anatase phase (Niederberger, 2002). The material has many uses such as gas sensors, dielectric ceramics, catalysts for thermal or photoinduced processes, photovoltaic solar cells, and pigments(Niederberger, 2002). One large market for $TiO_2$ is sunscreen products. The high scattering and absorption of $TiO_2$ results in screening of otherwise potentially harmful solar radiation.

$TiO_2$ NPs have been synthesized by a wide variety of routes. Some are based on hydrolyzation of titanium halides (Holmberg, 2012) or nonhydrolytic reactions with alcohols (Niederberger, 2002), others use sol-gel processes with metal alkoxides (Yoldas, 1986). Many of these reactions are very rapid and controlling the growth in size and shape can be problematic. For

many applications it is preferable to have particles with a narrow size distribution and well-defined morphology to give accurate results.

# Analytical methods

## Transmission Electron Microscopy (TEM)

TEM is a method using the transmission of electrons to image a material. This electron microscope uses the electron's short wavelength to achieve a very high resolution, which makes TEM a useful tool to resolve small features of a material. The electron gun is aimed directly at the sample and the electrons that pass through the sample are recorded. This gives information about the inner structure of materials, but gives a restrictive limit on sample thickness. Due to the extremely small particles in this project, the TEM has been an invaluable tool to evaluate the formed materials, giving information about particle size, morphology, and distribution. Moreover, with the help of dark-field imaging the crystallinity of particle can be examined. The instruments used in this project were *JEOL 1200 EX TEM* and *FEI Tecnai T20 LaB6 ST*

## Scanning Electron Microscopy (SEM)

In this project, SEM coupled with energy dispersive x-ray spectroscopy (EDX) was mainly used to verify the particle composition and ensure the incorporation of hafnium within NPs. Similar to TEM, SEM also uses electrons to surpass the resolution limit of visible light. However, for imaging SEM detects scattered and secondary electrons instead of transmitted ones. While not quite as highly resolved as TEM, the scanning feature of SEM makes it a very powerful technique to image surface topography. The SEM instrument used was a *Leo Ultra55 FEG.* The EDX feature is available both in SEM and TEM instruments.

## X-ray diffraction (XRD)

XRD is a characterization method utilizing the scattering of x-rays when a beam passes through a crystalline material. It is based on the Bragg's Law, which is a relation between angle and wavelength. This method gives information about crystalline structure such as d-spacing and also to some extent the composition of crystalline materials. The diffraction pattern obtained for a sample can be correlated for that of pure materials. Due to the irregularity in amorphous samples they give characteristic spectra with peaks at every angle. An example of this can be seen in figure 9.

## Dynamic Light Scattering (DLS)

DLS is a common method to analyze hydrodynamic radius and size distribution of particles in dispersion. It can be applied to many different materials, such as polymers, proteins or as in this case a metallic oxide. It uses spectral analysis to determine size down to the nanoscale range. The principle of the technique is to study the scattered light when passed through a colloidal systems. A basic DLS setup schematic can be seen in figure 1. When the particle size is smaller than the wavelength of the light; the scattering is called Rayleigh scattering. The DLS measures time-variation in scattering. This scattering is correlated to the Brownian motion of particles, which is dependent on particle size. It is not uncommon that NPs form larger agglomerates and DLS can be used to analyze if agglomeration is occurring. The information of particle size gives a statistical view of the size distribution which TEM cannot accomplish. It is important to note that DLS measures the hydrodynamic size, which is slightly larger since it includes a layer of molecules around the surface. It also assumes a spherical sample so for rod shaped particles, the actual diameters are overestimated. The two DLS instruments used were an *ALV-CGS3* and a *Zetasizer Nano ZS*.

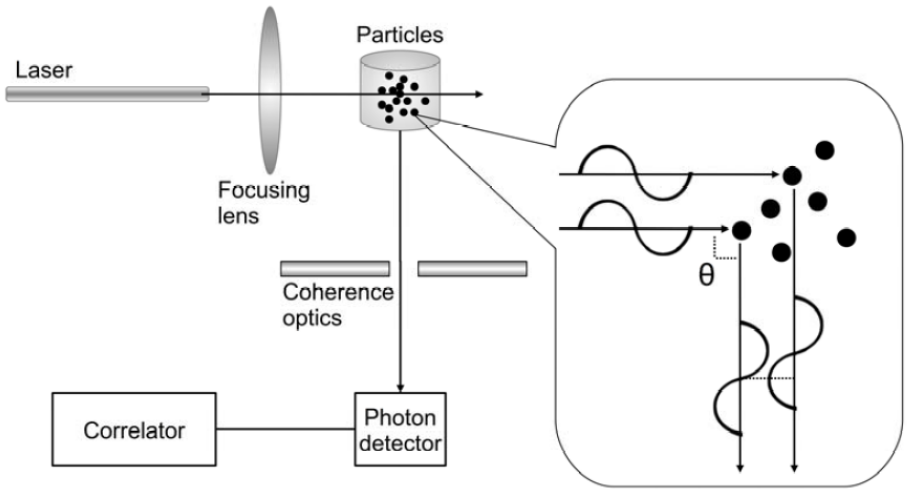


**Figure 1 – A schematic over the parts in a DLS-instrument with θ=90° (Holmberg, 2011)**

## Autoradiography

The aim of this project was to prepare particles suitable for use in autoradiography, which is a method using the emissions of decaying nuclides to image a sample. Basically it is analogous to an ordinary scanner. It is a sensitive technique, as every single decay can be detected depending on the half-life of the nuclide. Therefore, it is critical to find suitable radioactive markers. Emissions are detected and super-positioned over an image of the sample giving a precise localization method. A great advantage is that it is possible to use *in vivo* with $^{3}H$ or $^{125}I$ to trace things like biomolecules.

Titanium has no suitable isotopes for autoradiography, due to very short half-lives. The longest-lived isotope is $^{45}$Ti with a lifetime of about three hours and most of the rest in the range of fractions of seconds. This is far too low to be usable and so the particles have to contain another element. It is preferable to have a similar element to not alter the chemistry or structure of particles too much so the obvious first choices were Zirconium and Hafnium from the same group in the periodic system.

# Synthesis

## Hydrolysis Synthesis

The initial synthetic route chosen was based on the work of Jenny Perez Holmberg (Holmberg, 2011). This synthetic route is based on hydrolysis of titanium tetrachloride in water according to:

$$TiCl_4 + 2H_2O \rightarrow TiO_2 + 4H^+ + 4Cl^- \quad \text{Formulae 1}$$

A scheme of the synthesis implementation can be seen in figure 2. This synthetic route provided a way to produce TiO2 without the use of organic materials. Organic molecules tend to adhere to the surface of NPs and post-synthetic removal of impurities and surfactants can be very difficult. Since surface impurities might affect the result of later skin studies, a free surface would be preferable. The hydrolysis of titanium tetrachloride is very rapid, thus difficult to control, which is circumvented by using a low temperature. To control the particle size two factors are critical: temperature and ionic strength. The temperature can be varied in the dialysis and storage steps, while the ionic strength is controlled by the length of dialysis and water change frequency.

This synthetic route was abandoned in the beginning of the project due to unsatisfactory product. The product formed is a polymeric sol-gel network of O-Ti-O bonds and this network was then supposed to degrade into discrete NPs. This was not observed and so another synthetic route had to be chosen.

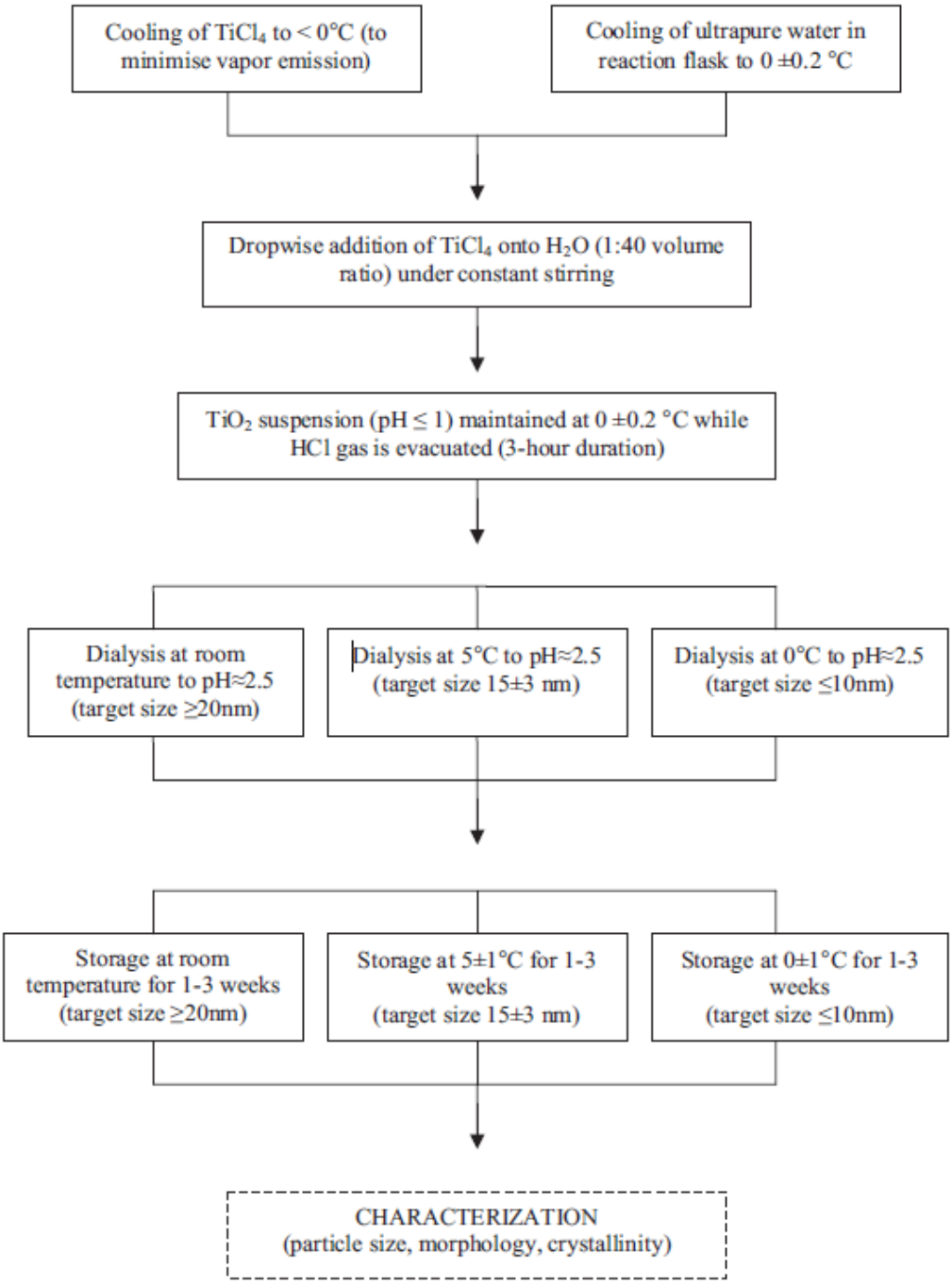


Figure 2 – Schematic of hydrolytic synthesis (Holmberg, 2011)

# Aminolysis synthesis

The aminolysis reaction chosen was based on the work of *Zhang et al (Zhang, 2005).* According to their article this system produces particles with a very narrow size distribution and also has the advantage of a variable aspect ratio. The used reactants are oleylamine ($CH_3(CH_2)_7CH=CH(CH_2)_7NH_2$), oleic acid ($CH_3(CH_2)_7CH=CH(CH_2)_7COOH$), and titanium isopropoxide ($Ti(OCH(CH_3)_2)_4$). Oleic acid will react with the titanium isopropoxide forming a stable titanium carboxylate intermediate, which together with oleylamine will form amides, according to figure 3, which then polycondensates to form TiO2 NPs. This can occur in two ways as illustrated in formula 2 and 3.

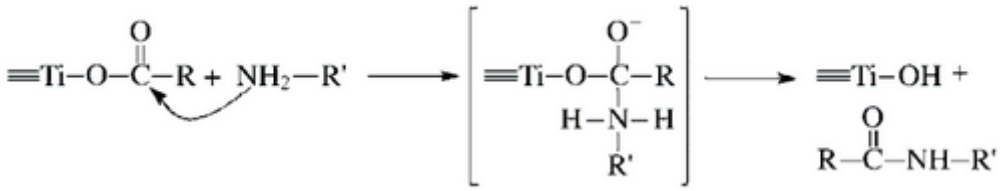

**Figure 3 – Aminolysis between carboxylated titanium compound and an amine, producing titanium hydroxide. (Zhang, 2005)**

$$M - OH + M - OR \rightarrow M - O - M + ROH \quad \textbf{Formulae 2}$$

$$M - OH + M - OH \rightarrow M - O - M + H_2O \quad \textbf{Formulae 3}$$

There are several controllable factors affecting the kinetics of the reaction, which in turn leads to a size difference of as-formed particles. The long, bulky hydrocarbon chains on oleic acid and oleylamine serve as a steric hindrance which significantly slows down the reaction. The temperature can be varied; in this case usually between 260°C and 300°C. Another important factor is the oleylamine amount, which accelerates the reaction and directly controls the shape of the particles.

The molar ratios between OLA, TIP and OA determine the shape of as-synthesized particles. A ratio varying from 5:1:1 to 5:1:4 gives 12nm rods, 30nm rods, 16nm rods and 2-3nm spherical particles (Zhang, 2005). The radius can be affected by addition of cetyltrimethylammonium bromide (CTAB), which acts as a weak capping agent.

The different samples formed in this work will be referred to with a simple code e.g. 30R-HfTi-G where 30 is the particle length, meaning 30nm rods, HfTi indicates it is after Hf has been

incorporated to the system and G or A indicates if it was produced using the Glassware or Autoclave setups.

A typical preparation of 30nm rods with scaled-up reagents (6-fold) can be described as follows:

1) 9.6ml OLA and 72ml 1-ODE were added to the reactor. It was then bolted onto the autoclave and the solution was stirred and degassed at 80°C for 1h.
2) 1.8ml TIP was injected into the solution and kept at 80°C for 20min and then heated up to 260°C where it was kept for 10 min.
3) 3.84ml OA was rapidly injected and let react for 1 h before cooling down to room temperature.
4) To clean the product and stop further reaction the resulting solution was diluted 1:2 with hexane and precipitated with twice as much acetone. Thereafter it was centrifuged to separate precipitated particles from the solvent. This procedure was done at least three times.

When Hf was introduced into the system it had to be dissolved in a separate beaker. Roughly one tenth of the amount of solvent together with one fourth of the OLA was degassed for 1 h. After sufficient degassing the hafnium isopropoxide was added (one tenth of the molar amount of titanium isopropoxide), it was stirred until completely dissolved and then added to reactor together with TIP in step 2.

The final recipe used for different particles:

**Table 1– The recipe for pure Ti Synthesis for different shapes of particles**

| | 1-ODE(ml | OLA(ml) | TIP(ml) | OA(ml) |
|---|---|---|---|---|
| 30R-Ti | 60 | 16 | 2.7 | 6.4 |
| 12R-Ti | 60 | 16 | 2.7 | 3.2 |
| 2.3S-Ti | 60 | 16 | 2.7 | 12.8 |

**Table 2– Variation of oleylamine for different expected shapes of particles**

| | 1-ODE(ml) | OLA(ml) | TIP(ml) | HfIP(g) | OA(ml) |
|---|---|---|---|---|---|
| 30R-HfTi | 60 | 16 | 2.7 | 0.4146 | 6.4 |
| 12R-HfTi | 60 | 16 | 2.7 | 0.4146 | 3.2 |
| 2.3S-HfTi | 60 | 16 | 2.7 | 0.4146 | 12.8 |

Two different reactors were used for the aminolysis synthesis. Initially an autoclave used for high pressure and temperature studies was used. The advantage with this was an automatic temperature control system that allowed precise setting of the temperature, which is crucial

for this application. It also had a build in stirring and gas lines for degassing with nitrogen. There also proved to be several downsides with this system. The reaction takes place near the boiling point of the solvent, so an effective reflux system would have been required. Since this was lacking, about half of the tried syntheses dried out. This might have to do with a thermometer problem which led to faulty temperature measurements when stirring or gas flow was high. This made the heating mantle increase heat to try to keep the temperature and thus increasing it to above 300$^{o}$C and thus boiling away the solvent. Another problem was that the product showed traces of sulfur, which should not have been present, and so to verify that the reactor setup was the source of this sulfur, a new glassware setup was assembled.

The glassware reactor, seen in figure 5, was a simple three-headed beaker with two splitters in it, giving the five openings needed for the synthesis. These were stirring, nitrogen inflow, injection, thermometer and gas outflow with a solvent reflux part to retain all solvent. To achieve the high temperatures needed for this synthesis a heating mantle was used together with quartz wool for isolation. Since everything was visible it was easier to see what happened and troubleshoot the process. The temperature was less exact however, possibly giving a source of variability of particle sizes between batches. Since the glassware was detachable it was easier to clean it completely giving less contamination than the previous setup.

One big advantage with this reactor was that the HfIP could be injected directly together with TIP, since the gas outlet could temporarily be removed and the powder could be poured inside. This might have given a better integration of hafnium into the particles, which was a concern earlier. It also simplified the synthesis better timing of all the steps.


**Figure 4 – Photograph of autoclave setup with the reactor off. The components are 1: Reactor 2: Heating mantle 3: Fitting for reactor 4: Sampling port 5: Nitrogen in 6: Nitrogen out**

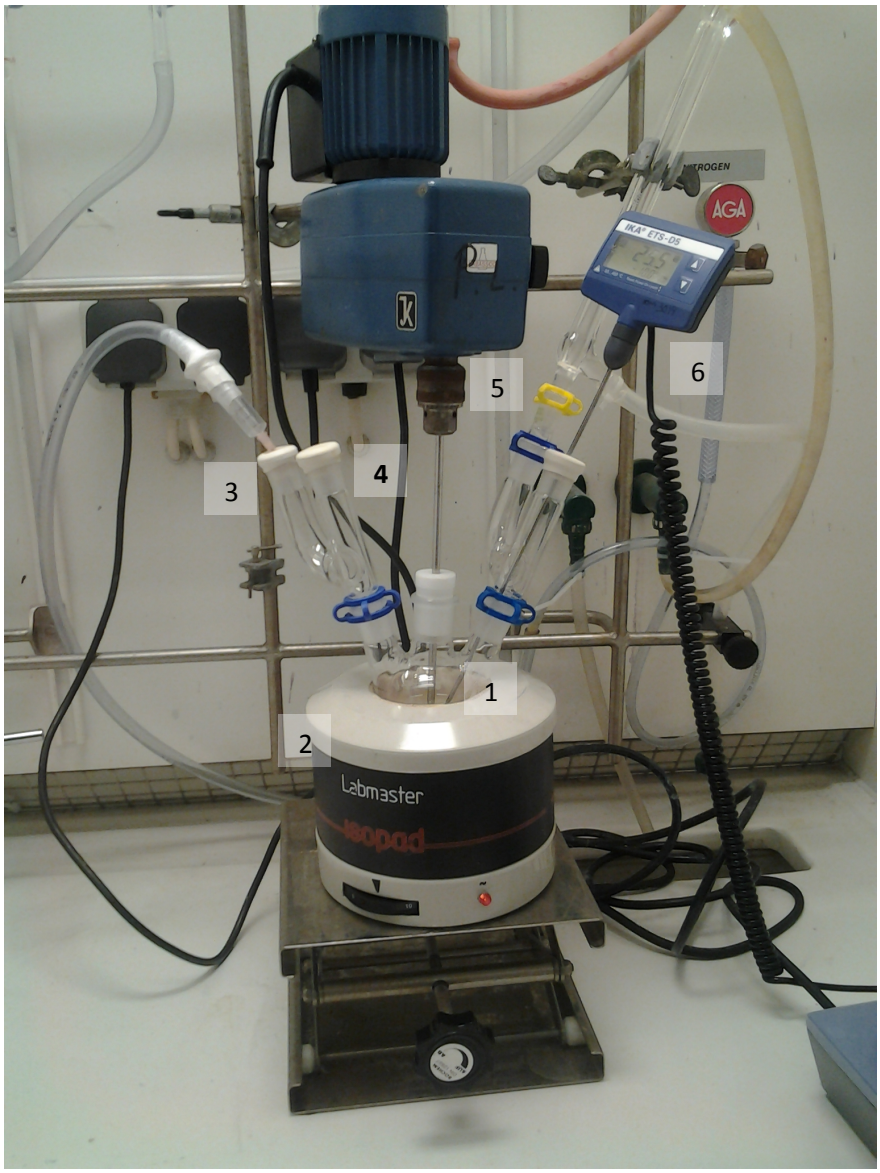


**Figure 5 – Glassware setup the components are 1: Reactor 2: Heating mantle 3: Nitrogen in 4: Injection opening 5: Stirring motor 6: Thermometer**

# Results

## Hydrolysis Reaction

For the first hydrolysis reaction, the dialysis step was skipped and thus aggregated particles were expected, however, directly after synthesis the product proved to be a mixture of colloidal network and aggregated particles, as shown in figure 6 and 7. The bright areas in the dark-field image to the right indicate crystalline regions within the aggregated particles. Upon storage in the mother solution, the colloidal network evolved into larger particles, as shown in figure 6 and 7. Crystallinity was presented in some big particles, as suggested by the dark-field images (Fig. 6 F, J, L). However this conversion was not well controlled, as particles with large size-distribution and irregular morphologies were observed.

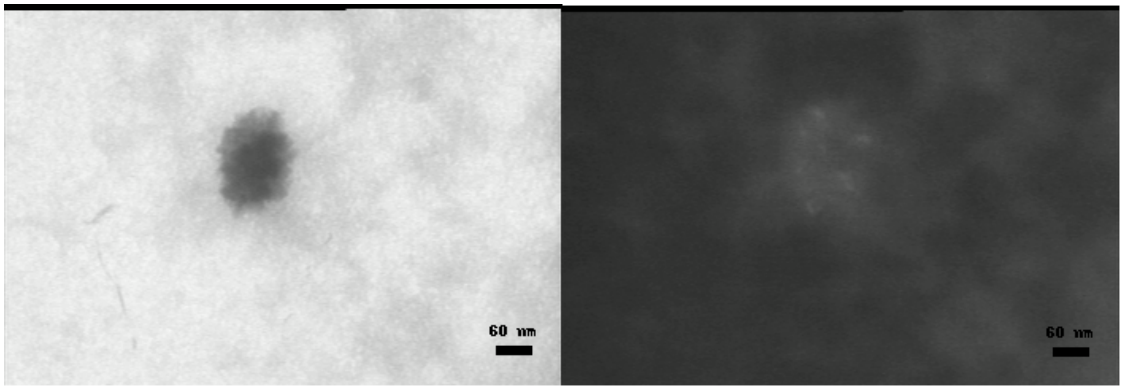


**Figure 6 – TEM micrographs of samples formed from Hydrolysis reaction 1 without dialysis: bright-field (left) and dark-field (right) image.**

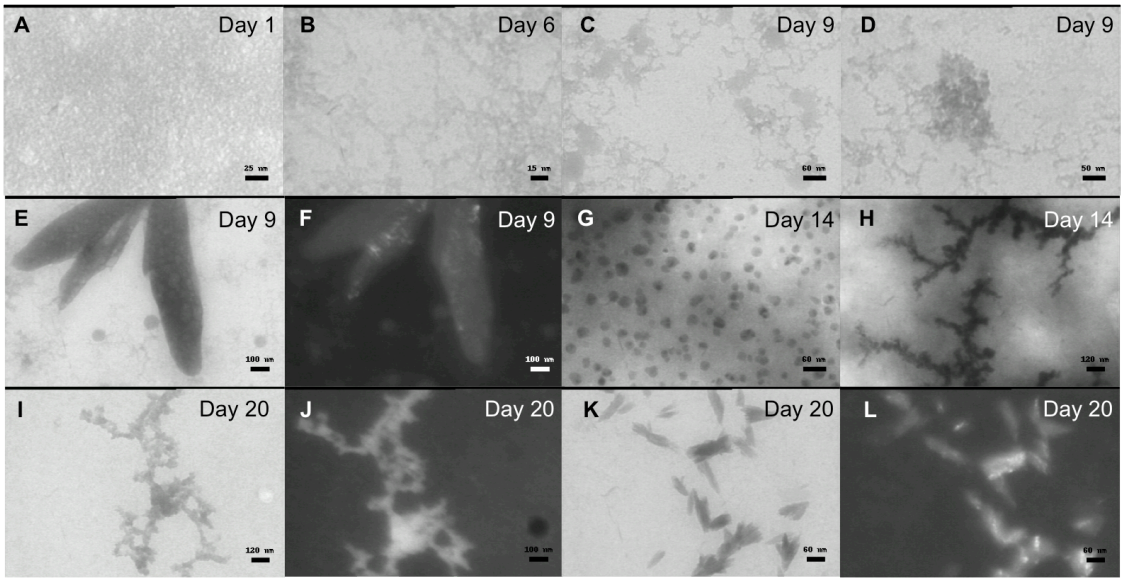

Figure 7 - TEM micrographs of samples formed from Hydrolysis reaction 1 (without dialysis) and with a storage time of 1 to 20 days. Figure F, J and L is the dark-field image of the same particles shown in E, I, and K respectively. Scale bars: A 25nm; B 15nm; C, G, K, L 60nm; D 50nm; E, F, J 100nm; H, I 120nm.

The second synthesis involved a dialysis step after reaction, and the product contained mostly the colloidal network (shown in figure 8 A) as observed from the first synthesis.

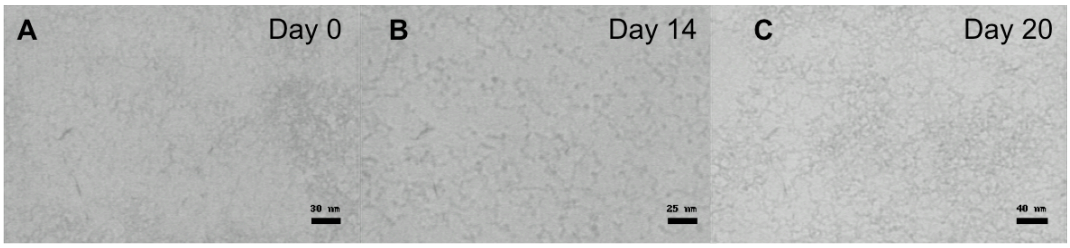


Figure 8 – TEM of samples from Hydrolysis reaction 2 after dialysis and with a storage time of 0 to 20 days. Scale bars: A 30nm; B 25nm; C 40nm.

Since the product seemed to exhibit mostly colloidal network and no small, well defined particles, XRD analysis was performed, which proved that the as-prepared network was amorphous, as seen in figure 9.

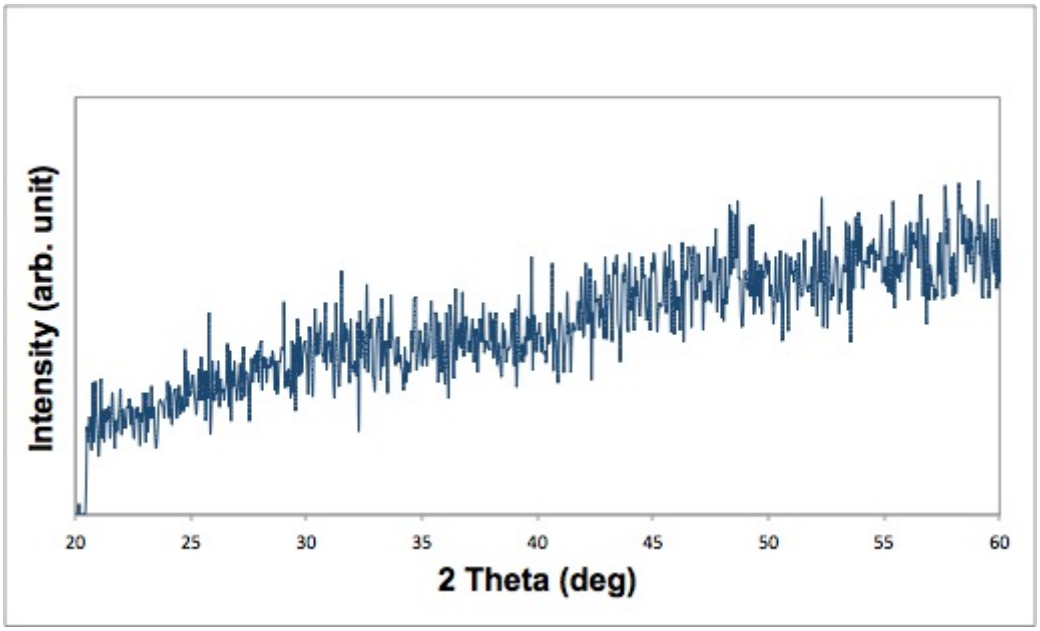


Figure 9 – XRD spectra of samples from Hydrolysis reaction 2 after dialysis.

The amorphous sol-gel product was expected but was supposed to slowly crystallize to NPs over one to three weeks, however no significant difference was observed during three weeks storage, as shown in figure 8, B, C. However, a few large agglomerates, which exhibited crystalline regions, were observed in the sediment in mother solution after 2 weeks of storage. An example of this can be seen in figure 10.

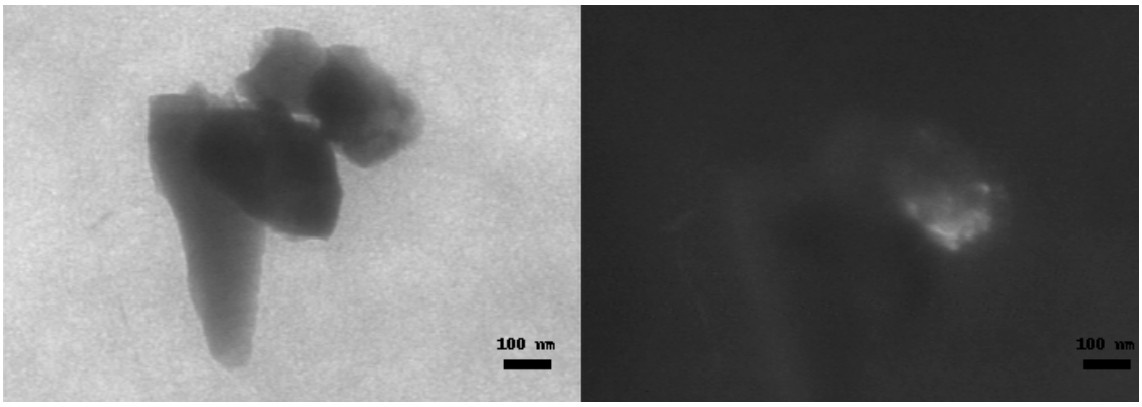


Figure 10 –TEM micrographs of samples formed from Hydrolysis reaction 2 after dialysis and stored for 2 weeks: bright-field (left) and dark-field (right) image.

## Aminolysis Reaction

The aminolysis reaction seemed more controllable and immediately gave particles for characterization. For the initial samples of pure $TiO_2$, TEM images seem to show rod-shaped particles of roughly the size expected. The dark-field analysis shown in fig. 11C supported the result by showing rod shaped crystallites as is seen in fig. 8. The diffraction pattern in figure 11 F also indicates crystallinity. The shape seems to be slightly elongated, but not quite 30nm. That does not necessarily mean so much due to the nature of TEM, which does not give a statistical view of the entire sample. Figure 11 D & E shows particles around areas of clear carbon film.

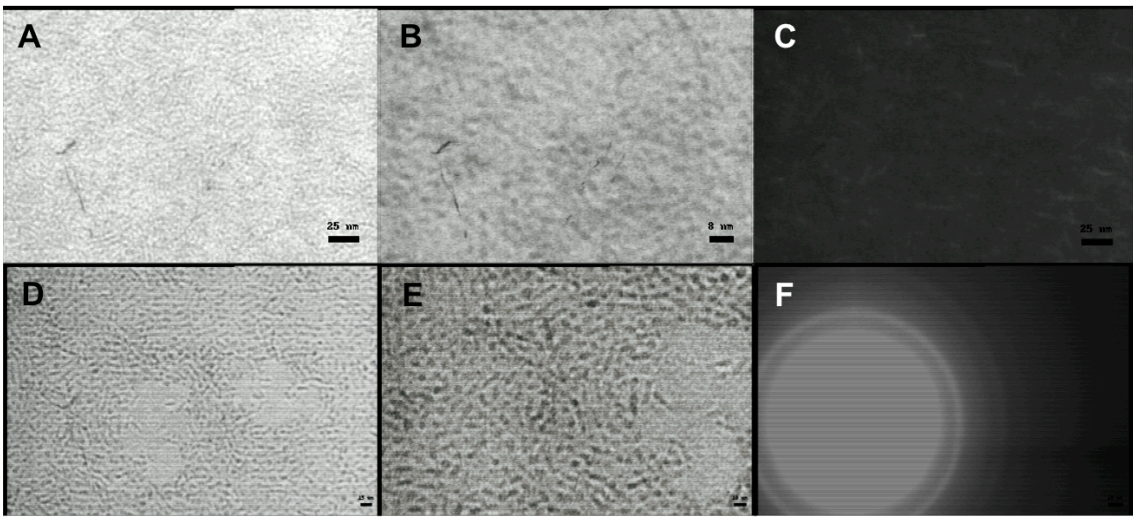


Figure 11 – TEM micrographs of pure $TiO_2$ rods (sample 30R-Ti-A) synthesized from autoclave reactor: A, B, D, E bright-field image; C dark-field image; F selected area electron diffraction. Scale bars: A, C 25nm; B 8nm; D, E: 15nm.

XRD analysis of a sample of pure $TiO_2$-rods synthesized by aminolysis in the autoclave reactor, seen in figure 12, showed a diffuse pattern that could be attributed to the anatase form of $TiO_2$

(Wang, 1999). However the broad diffraction peaks indicates the poor crystallinity of the sample, which is brought by the extremely small particle sizes.

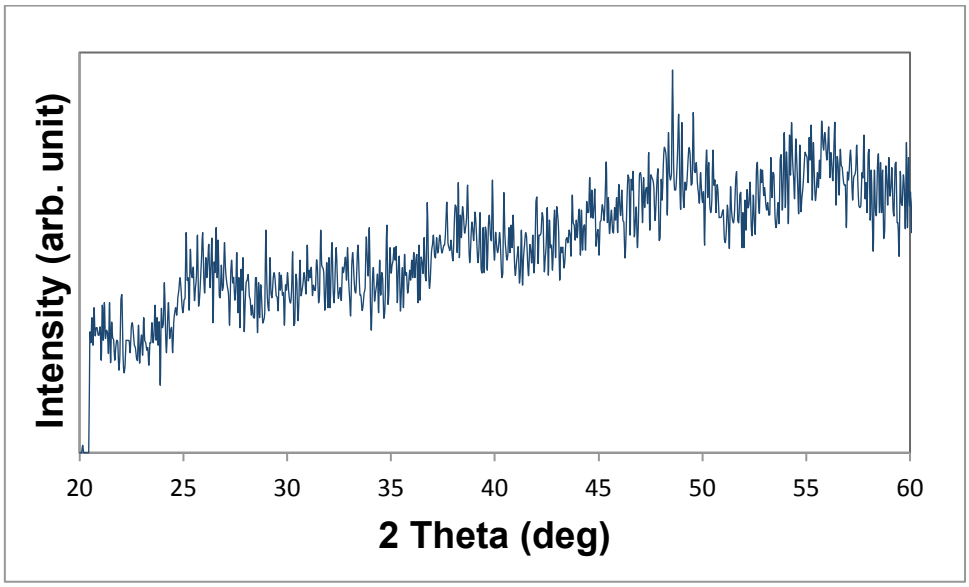


**Figure 12 – XRD spectra of $TiO_2$ sample from aminolysis reaction in autoclave reactor. Sample 30R-Ti-A**

After the inclusion of Hf in the synthesis a clear shift in particle shapes can be seen. Figure 13 shows TEM images of autoclave syntheses with Hf. Figure 13 A & B is from a 30nm rod synthesis, however the particles seem less elongated and with a wider size distribution than previously exhibited. Figure 13 C is from a 12nm rod synthesis with Hf where the particles seem more or less spherical. D shows particles from a sphere synthesis and while they seem spherical the features are difficult to resolve with the JEOL 1200 EX TEM instrument.

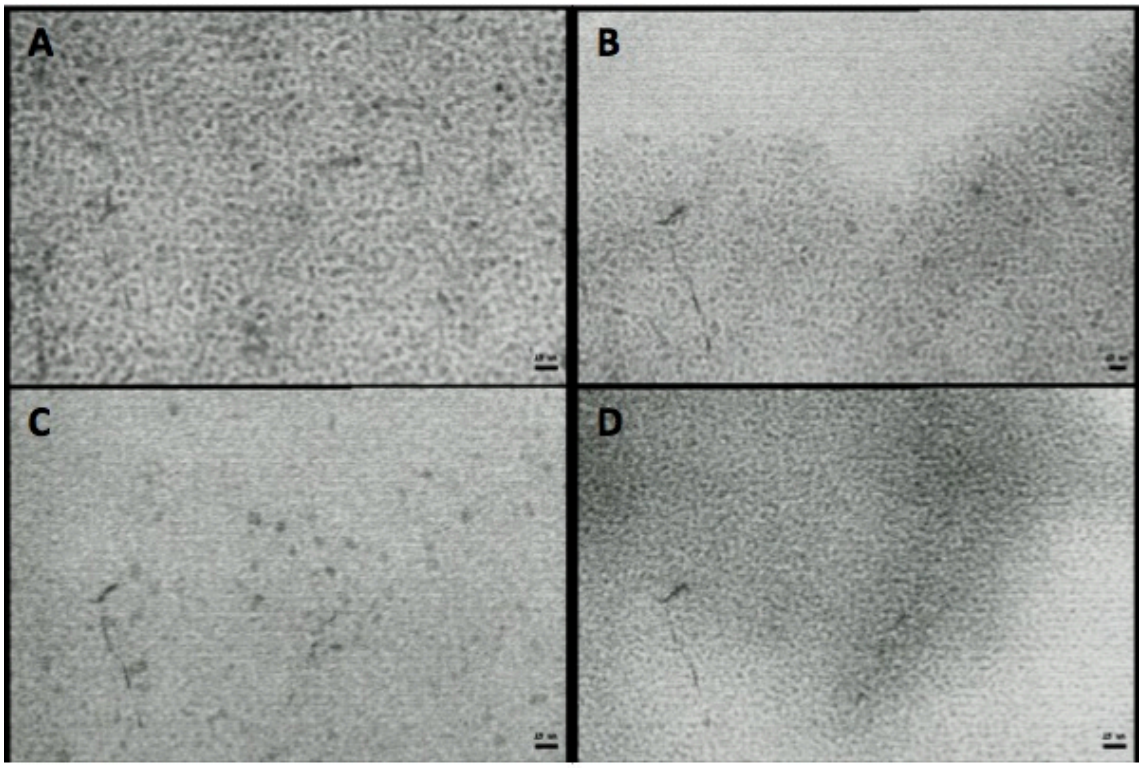


Figure 13 – TEM micrographs of Hf-doped $TiO_2$ samples synthesized from autoclave reactor: A, B sample 30R-HfTi-A; C sample 12R-HfTi-A; D sample 2.3S-HfTi-A. Scale bars: A-D 15nm.

Using DLS to measure the particles in dispersion showed a relative narrow size distribution and very small size. In Figure 14 – DLS spectra of three samples, one sphere sample with Hf and two 30-nm rod samples with and without Hf.figure 14 the number average radius is shown to be around 2-3nm.

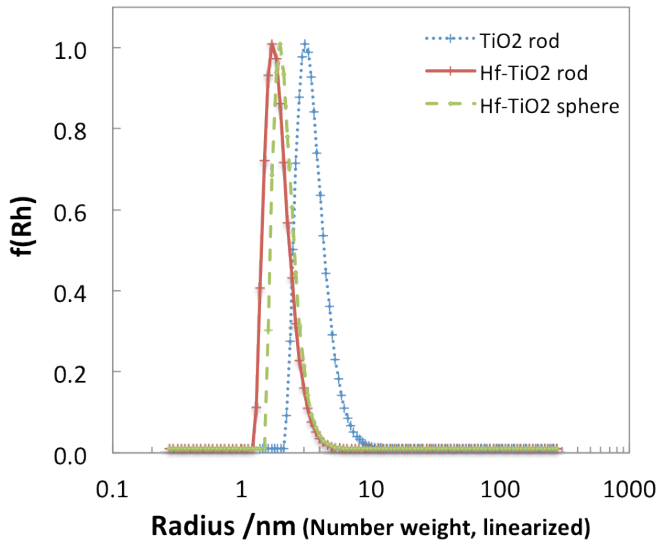


Figure 14 – DLS spectra of three samples, one sphere sample with Hf and two 30-nm rod samples with and without Hf.

The result from EDX analysis performed on the three different variations for the autoclave synthesis is presented in figure 15-17. The contents look quite similar, even though the size of the peaks varies. The expected peaks of C, Cu, Ti, O are present and Hf is also present in all the samples.

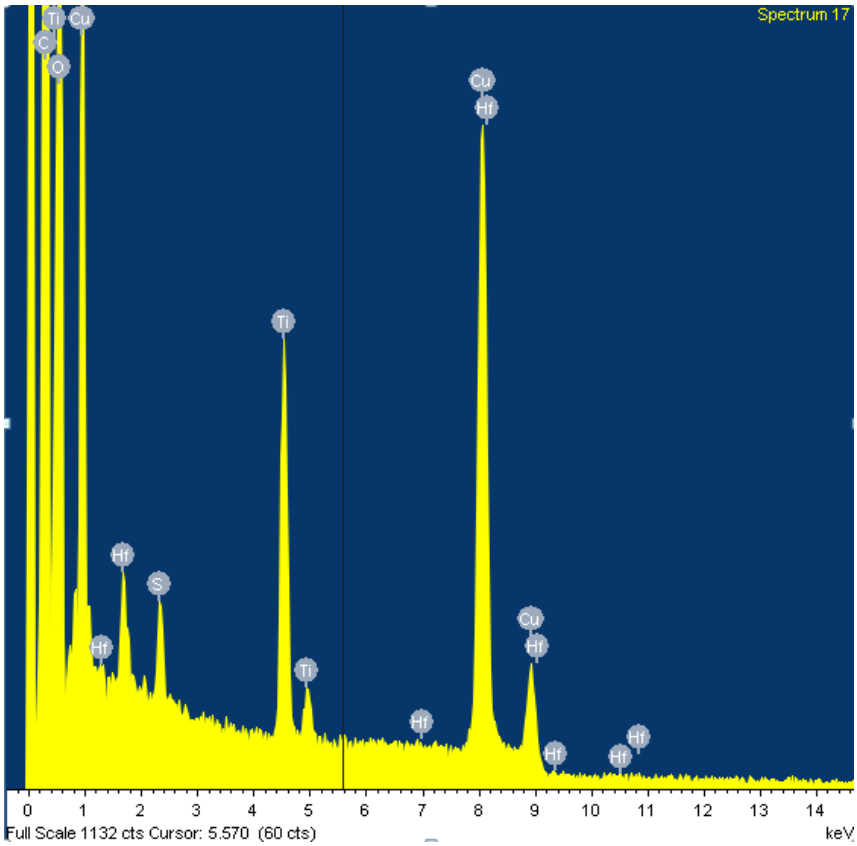


Figure 15 – EDX spectra for 2.3S-HfTi-A

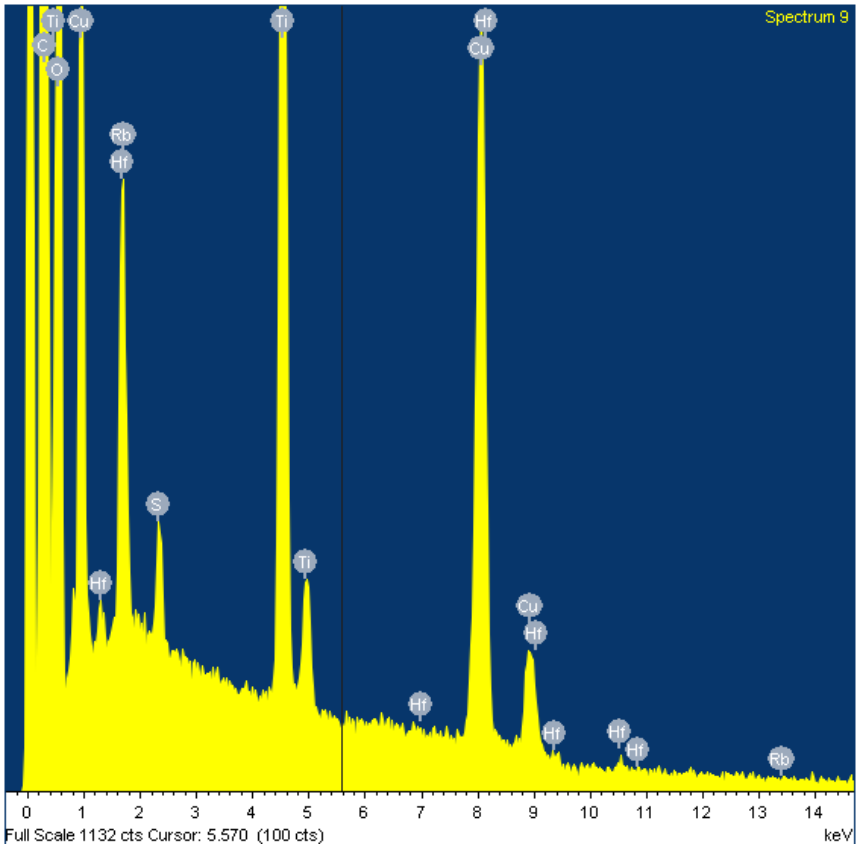


Figure 16 – EDX spectra for 30R-HfTi-A

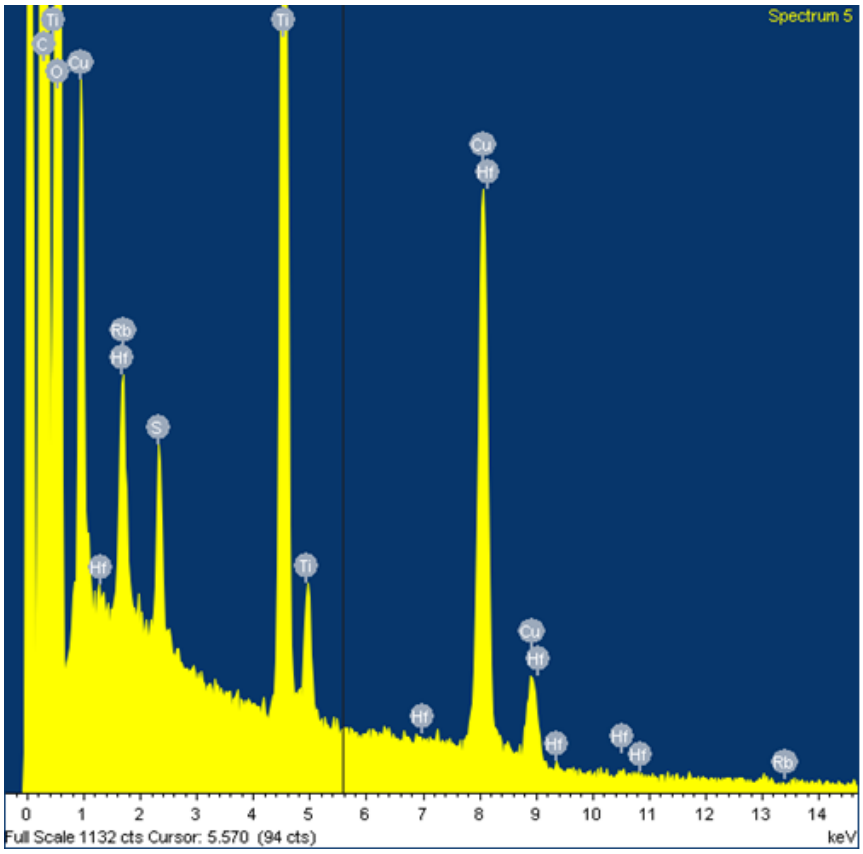


Figure 17 – EDX spectra for 12R-HfTi-A

In table 3 a summary of the atomic percentage of different elements is presented. Important to note is that for the Hf measurement both Ta and Rb are assumed to be Hf as well, due to the unlikelihood of them being present in the samples. Therefore these values were added to Hf here.

**Table 3 – Table of atomic % of elemental composition of autoclave syntheses.**

| Atomic % | 30R-HfTi-A | 12R-HfTi-A | 2.3S-HfTi-A |
|---|---|---|---|
| C | 80.88 | 78.01 | 80.95 |
| O | 15.44 | 18.37 | 16.43 |
| S | 0.08 | 0.08 | 0.08 |
| Ti | 1.01 | 1.84 | 0.46 |
| Cu | 2.39 | 1.5 | 2.04 |
| Hf | 0.35 | 0.19 | 0.04 |

In figure 18 the resulting TEM micrographs for glassware synthesis can be seen. A & B are 30R-samples. It is possible to see rod shaped particles with approximately the expected shapes. The size distribution seems better than for autoclave syntheses. C & D show 12R-samples. The particles are slightly less elongated than those in A & B. To the left of image C is a clear area of carbon film. E & F are images from 2.3S-synthesis and the particles are hard to see. Due to the small shape it is possible they are lost in the features of the carbon film from the sample grid.

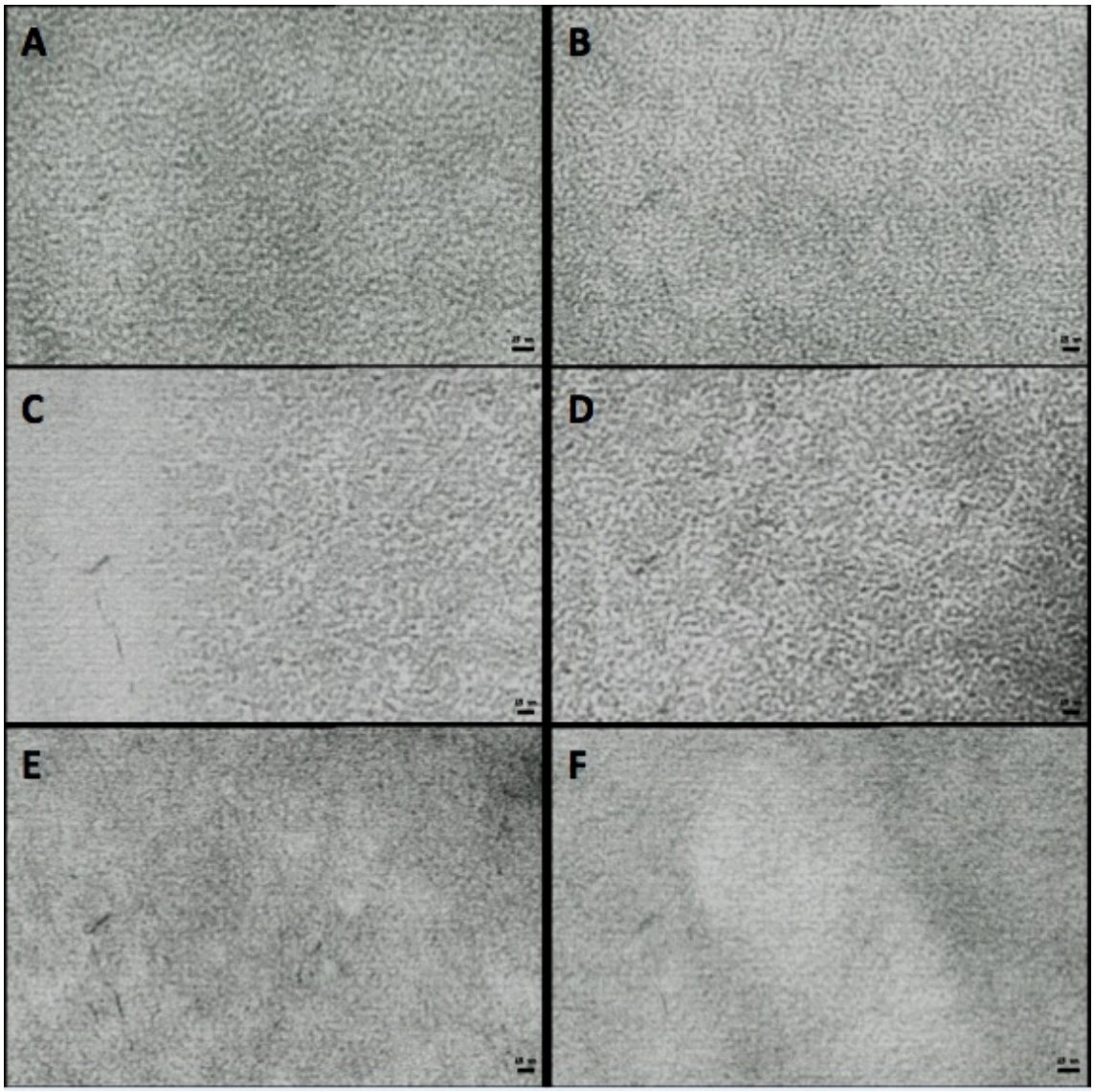


**Figure 18 – TEM micrographs of Hf-doped $TiO_2$ samples synthesized from glassware reactor: A, B sample 30R-HfTi-G; C, D sample 12R-HfTi-G; E, F sample 2.3S-HfTi-G. Scale bars: A-F 15nm.**

The samples were also analyzed using a FEI Tecnai T20 LaB6 ST TEM instrument with a higher resolution than the JEOL 1200 EX TEM used above. In figure 19, images for the 12R-HfTi-G and 30R-HfTi-G samples are shown. Due to the very high resolution the individual lattice planes can be seen, surrounded by what looks like amorphous domains or possibly the carbon film on the sample grids used. The crystalline regions do not match the expected particle length, possibly because of low crystallinity in the sample.

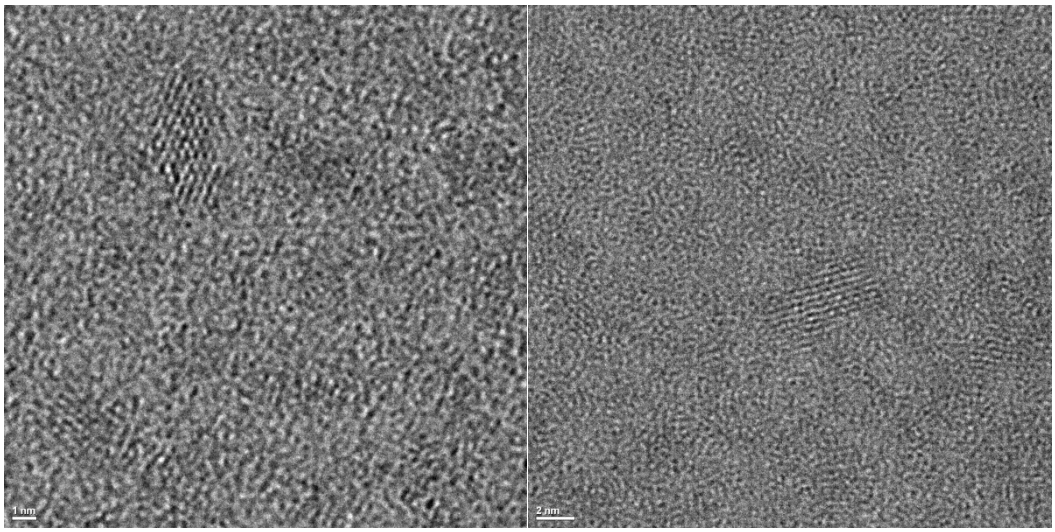


**Figure 19 – TEM micrograph of visible lattice planes for a 12R-HfTi-G sample to the left and 30R-HfTi-G to the right. Scale bars: Left 1 nm, right 2 nm**

Using this instrument an EDX analysis was also performed and the samples exhibited more or less expected elemental composition with large amounts of titanium, oxygen and hafnium, which can be seen in figure 20. There was still sulfur present but in lower amounts than for earlier samples from autoclave synthesis.

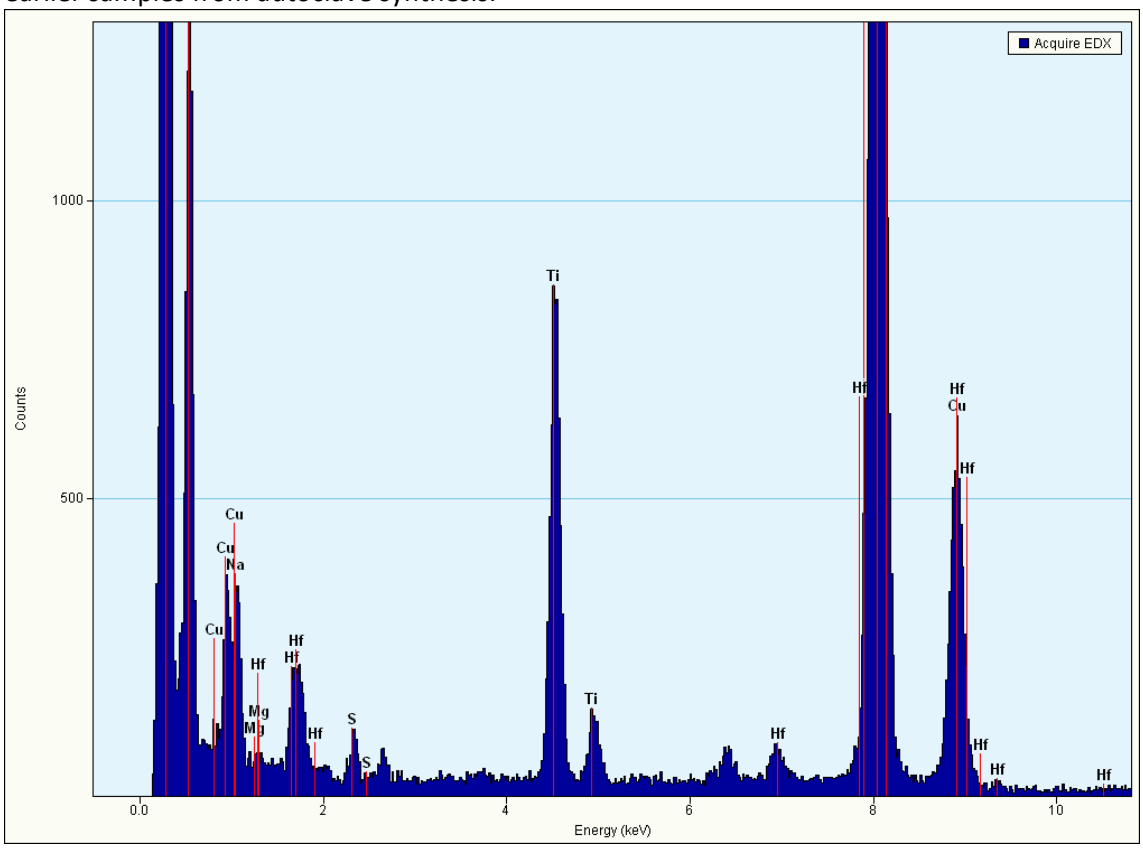


**Figure 20 – EDX analysis of 30R-HfTi-G sample**

Further analysis of HfTi-G samples using DLS showed number average diameters around 10nm where 30R was slightly above and 12R was slightly below. This supported the presumption of a larger equivalent sphere for longer rods and thus also contradicted the result from previous DLS. This is shown in table 3 and the size distributions can be seen in figure 21 and 22. The 2.3S

sample yielded no result. This is either because the particles were below the detection range or that they did not re-disperse and thus yielded no result.

Table 4 – Diameters from DLS on HfTi-G samples

| Diameters | Z-avg[nm] | n-avg. [nm] |
|---|---|---|
| 30R-HfTi-G | 43,95 | 11,85 |
| 12R-HfTi-G | 41,55 | 8,35 |
| 2,3S-HfTi-G | No result | No result |

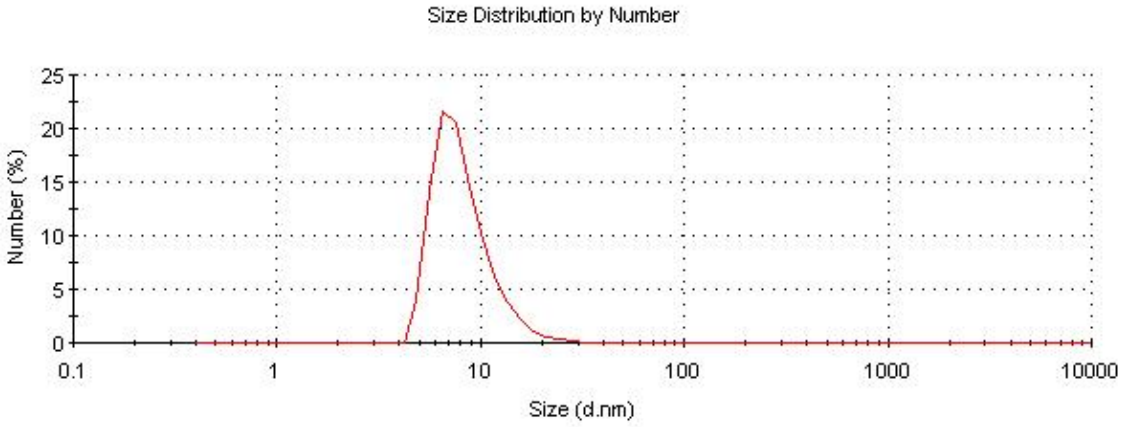


Figure 21 – Size distribution by number from DLS for 12R-HfTi-G

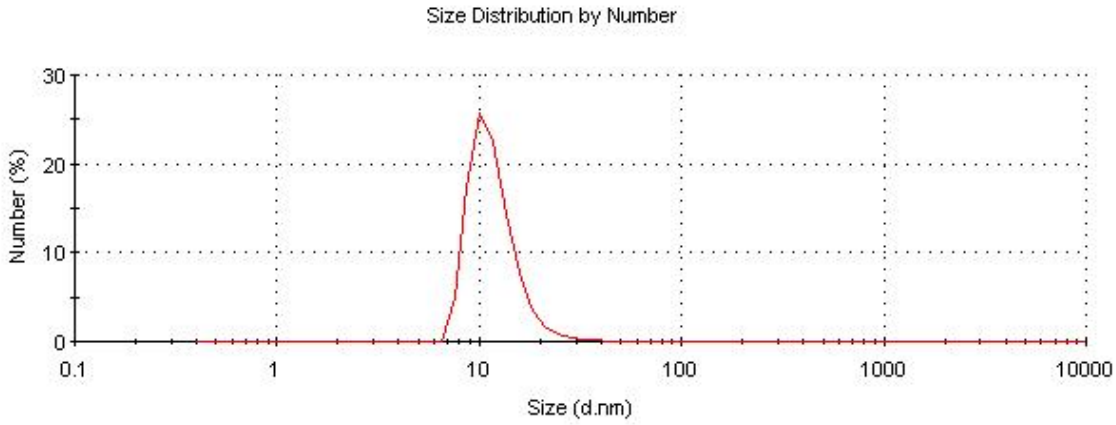


Figure 22 – Size distribution by number from DLS for 30R-HfTi-G

# Discussion

The initial synthesis using hydrolysis of $TiCl_4$ proved to yield no nanoparticles at all, instead an amorphous sol-gel was formed. In some areas this sol-gel formed crystalline regions however these were not in the desired nanoscale range. Over the course of 20 days the degree of crystallinity increased as is illustrated in figure 7, where this transition can be seen. The difference between using dialysis and not was also observed and for samples after dialysis no significant change over time was noticed. The dialysis step reduces ionic strength in the solution by removing the chloride ions released by the hydrolysis of $TiCl_4$ (Holmberg, 2011). By lowering the ionic strength the formation of crystalline regions should slow down and form smaller particles, so it is possible the sample would eventually have shown the desired structures but a storage time of over three weeks can be impractical. It is also possible that hydrothermal treatment or calcination would have induced crystallinity in the samples.

For the aminolysis reaction for pure $TiO_2$ the two different setups seemed to significantly affect the shape. Although the recipes followed were identical, the autoclave setup lacked any reflux and often ended with at least half the solvent evaporated. The control of particle shape was also better when comparing results for pure $TiO_2$ syntheses, which can be seen if comparing figure 13 and figure 18. This seems to indicate that the solvent amount is important for the formation of crystalline particles and that the reflux system in the glassware setup is quite important to achieve rod-shaped particles.

The two setups varied significantly in the Hf-addition step. To be able to add Hf to the autoclave it had to be dissolved first, which proved difficult. It had to be heated separately in solvent and oleic acid for around 1 h before addition. This difference in preparation might have had a significant effect on the end-product in favor of the autoclave, but after addition of Hf neither synthesis yielded products with as defined particles with narrow size distributions. The addition of Hf into the system might affect particle growth in a negative way.

An important reason the glassware reactor was used in the first place was the presence of sulfur in the system when the autoclave was utilized. This was assumed to come from the autoclave since previous users had used hydrogen sulfide gas in it. Comparing the EDX results from figure 20 and table 3, sulfur did not completely disappear from the product from the glassware setup but it was far lower than previously. Another important piece of information

from the EDX measurements was that Hf was actually present in the sample, however it is not possible to say if Hf and Ti are segregated to different regions or not. One indication that the Hf is actually incorporated into the $TiO_2$ structures is the alteration in particle shape.

The DLS measurement results presented in figure 14 show that the two Hf syntheses have a smaller diameter than the pure $TiO_2$ synthesis which does not agree with previous measurements. It also shows that the 30nm rod sample has a smaller diameter than the spheres which was not predicted, since the equivalent sphere diameter of the rod shaped particles should show a significantly larger diameter. A later DLS measurement performed on re-dispersed samples after pulverization compared 12nm rods with 30nm rods. The sphere sample yielded no usable result. For this measurement the 30R showed a larger diameter than 12R which corresponded to the prediction of the equivalent sphere model.

# Conclusions

The time constraint of doing a master's thesis limited this project and so the planned later stages were not completed. Particles with varied shape and doped with hafnium were synthesized and sent to irradiation. The reason for the significant delay was mostly that the particles were very difficult to accurately characterize. Another factor was that synthesis of the particles was highly unreliable in several ways. The hydrolysis reaction did not produce any NPs at all, which forced a restart with an entirely new synthesis, even though the absence of organic molecules on the particle surface would have been beneficial to the later stages of the project. The second synthetic route was more successful, however the first setup was lacking in a few ways. It leaked solvent and the automatic temperature control was not satisfactory leading to overheating. This led to a lot of wasted time, since each synthesis took roughly a day of work. The most successful setup was the glassware setup which was easier to control due to the fact that it was visible, the temperature was manually controlled and the system could be thoroughly cleaned to minimize contamination.

The particles produced were difficult to characterize using TEM, due to a very high translucency. In the later stages of the project a way around this was worked out. It would be of interest to continue to develop the characterization further to verify that the particles actually have the shape specified. The DLS proved to be a powerful instrument to see how narrow the size distribution was, but the exact diameter might not be very accurate. Initially DLS measurements did not correspond to the predicted pattern where spherical particles have lower diameters than rods. This changed in the later stages where 30R showed larger diameters than 12R. Since these are only two measurements with different instruments, performed in the lower ranges of detection, the results are not conclusive.

# Future works

Due to the time constraint of a master's thesis project all the goals set up at the beginning were not met, and so the obvious continuation of this work is to actually complete it. A set of particles has been sent away for irradiation and will be used to study the skin penetration in a near future. It would also be of interest to develop particles of more sizes and shapes to widen the range of study since the commercially used $TiO_2$ NPs are generally of a very large size distribution.

Furthermore there has been interest in using these particles to study the toxic effects in aquatic life, using the model organism zebra fish. Due to the resilience of $TiO_2$ as a material, a bioaccumulation of NPs could have negative impact on the environment and should therefore be studied.

# References


Cademartiri L, Ozin GA (2009) Concepts of Nanochemistry. *WILEY-VCH Verlag GmbH & Co.*

Holmberg JP, Abbas Z, Hellstrom AK, Hagstrom M, Bergenholtz J, Hassellov M, Ahlberg E (2011) Synthesis, characterization and particle size distribution of TiO2 colloidal nanoparticles. *Colloids and surfaces A – Physicochemical and engineering aspects*, vol 384, pp. 254-261

Krug, H.F., Wick, P. (2011) Nanotoxicology: an interdisciplinary challenge. *Angewandte Chemie. Int. Ed Engl.* 50, 1260-1278

Lee JE, Chung K, Jang YH, Jang YJ, Kochuveedu ST, Li DX, Kim DH (2012) Bimetallic Multifunctional Core@Shell Plasmonic Nanoparticles for Localized Surface Plasmon Resonance Based Sensing and Electrocatalysis. *Analytical Chemistry*, 2012, vol 84 (15), pp 6494–6500

Mortensen LJ, Oberdörster G, Pentland AP, DeLouise LA (2008) In vivo skin penetration of quantum dot nanoparticles in the murine model: the effect of UVR. *NANO LETTERS*, vol 8, pp 2779-2787

Nel A, Xia T, Madler L, Li N (2006) Toxic potential of materials at the nanolevel. *Science*, 311(5761), 622–627

Niederberger M, Bartl MH, Stucky GD (2002) Benzyl alcohol and titanium tetrachloride – a versatile reaction system for the nonaqueous and low-temperature preparation of crystalline and luminescent titania nanoparticles. *Chemistry of materials*, vol 14, pp 4364-4370

Sanders K, Degn LL, Mundy WR, Zucker RM, Dreher K, Zhao BZ, Roberts JE, Boyes WK (2012) In Vitro phototoxicity and Hazard Identification of Nano-scale Titanium Dioxide. *TOXICOLOGY AND APPLIED PHARMACOLOGY,* vol 258(2), pp 226-236

Schulz J, Hohenberg H, Pflucker F, Gartner E, Will T, Pfeiffer S, Wepf R, Wendel V, Gers-Barlag H, Wittern KP (2002) *ADVANCED DRUG DELIVERY REVIEWS,* vol 54, pp157-163

Thurn KT, Paunesku T, Wu A, Brown EM, B Lai, S Vogt, J Maser, M Aslam, V Dravid, R Bergan, GE Woloschak (2009) Labeling TiO2 nanoparticles with dyes for optical fluorescence microscopy and determination of TiO2-DNA nanoconjugate stability. *SMALL*,vol 5(11), pp 1318-1325

Wang CC, Ying JY (1999) Sol-gel Synthesis and Hydrothermal Processing of Anatase and Rutile Titania Nanocrystals. *Chemistry of materials*, vol 11, pp 3113-3120

Yoldas BE (1986) Hydrolysis of titanium alkoxide and effects of hydrolytic polycondensation parameters. *Journal of materials science*, vol 21, pp.1087-1092

Zhang Z, Zhong X, Liu S, Li D, Han M (2005) Aminolysis Route to Monodisperse Titania Nanorods with Tunable Aspect Ratio. *Angewandte Chemie-International Edition*, vol 44, pp.3466-3470